C. R. Mecanique 345 (2017) 208–220

Contents lists available at ScienceDirect

Comptes Rendus Mecanique

www.sciencedirect.com

# Vibro-acoustic modeling and validation using viscoelastic material

Rogério Pirk [a,*], Stijn Jonckheere [b,1], Bert Pluymers [b,1], Wim Desmet [b,1]

[a] Institute of Aeronautics and Space/Technological Institute of Aeronautics, Praça Marechal Eduardo Gomes, 50, CEP 12228-904, São José dos Campos, Brazil
[b] KU Leuven, Department of Mechanical Engineering, Celestijnenlaan 300, B-3001, Heverlee, Belgium

ARTICLE INFO

*Article history:*
Received 16 November 2016
Accepted 4 January 2017
Available online 6 February 2017

*Keywords:*
Vibro-acoustics
Passive control technique
Viscoelastic material
Finite element method
Fractional derivative method

ABSTRACT

In aerospace industries, on-board electronics are carried during flight, and such equipment must be qualified to withstand the loads to which they are exposed. In this fashion, the knowledge of the different dynamic aspects of excitations and the behavior of structures, components and/or acoustic enclosures are crucial to have controlled and performing space systems. Passive control techniques using viscoelastic materials (VEM) are widely applied and their effects on space systems must be studied aiming to obtain adequate operational environments. The effect of damping insertion on the dynamic behavior of a vibro-acoustic system is assessed in this work. A coupled structural–acoustic system, composed by a VEM coated aluminum panel and an acoustic box, is modeled by Finite Element Method (FEM). On the other side, tests are preformed using the KU Leuven facilities to validate the FEM model. Numerical vs. experimental comparisons were done and acceptable agreement was obtained. On the other side, it was found that sound inside the box reduces due to the smaller sound radiation generated by the treated panel.



## 1. Introduction

Expendable launch vehicles (ELV) carry payloads and electronics inside fairings and bays and such equipment must withstand the dynamic environment to which they are submitted. During flight, ELV experience loads from acoustic noises at lift-off, transonic and maximum dynamic pressure flights as well as vibration due to motors operation up to mechanical shocks generated during stage separations. Along the many years developing space systems, one could verify that these dynamic loads are characterized as highly intense, random and with large spectral contents. However, it is well known that qualification processes of space systems have high costs if intense dynamic levels are required. As a consequence, such an intense levels to which on-board equipment are exposed must be suppressed or attenuated.

The knowledge of the different dynamic aspects of excitations and the behavior of structures, components and/or acoustic enclosures are crucial to have controlled and performing space systems. Virtual prototyping supported by vibro-acoustic solutions is a significant tool to be used on space system developments, due to the proven cost benefits reflected into projects. Low-frequency deterministic methods such as Finite Element Methods (FEM) [1] and Boundary Element Methods (BEM) [2] have, due to increasing computer speed, been able to run deterministic models to higher and higher frequencies,

* Corresponding author.
*E-mail address:* rogeriorp@iae.cta.br (R. Pirk).
[1] Member of Flanders Make.

http://dx.doi.org/10.1016/j.crme.2017.01.001
1631-0721/

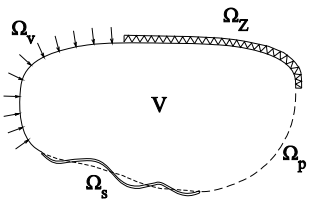


**Fig. 1.** Vibro-acoustic system.

while Statistical Energy Analysis (SEA) [3] has become an accepted method for both acoustic and vibration high-frequency analysis. One still may highlight mid-frequency methods as Wave Based Method (WBM) [4] and hybrid techniques (e.g., FEM/SEA) [5], among others.

The novelty in structures and materials and the increasing complexity of systems require new and more accurate numerical formulations as well as experimental validation procedures, to study their mechanical characteristics. Although computer models have evolved substantially, there are still many open issues, which impair design engineers to fully exploit virtual design processes. Nowadays, the demand on numerical simulations is high in the field of Noise and Vibration Harshness (NVH), e.g., the numerical modeling of multi-layer trim acoustic material and structural damping, largely used to attenuate air- and structure-borne noise. Structural damping insertion using viscoelastic materials (VEM) is a well-known passive control technique, widely applied in the aerospace industry. On the other side, the use of blankets or poro-elastic materials is spread as air-borne noise control technique. However, accounting vibro-acoustic systems, the structural noise radiation can be considered as an additional portion, when acoustic responses must be attenuated. In this framework, the effect of VEM insertion on the acoustic responses of coupled vibro-acoustic systems seems to be an appropriate assessment.

There is a significant motivation in the space industry to study sandwich structures (e.g., homogeneous panel + constrained VEM), since these systems present good NVH controlling performances as well as cost-effective mounting designs. This work focuses on the vibro-acoustic modeling of the KU Leuven Sound Box and an aluminum homogeneous plate treated with a VEM damper. In order to well characterize the frequency-dependent shear behavior of the VEM compound, measurement procedures using Dynamic Mechanical Analysis (DMA) and Differential Scanning Calorimetry (DSC) tests are applied [6]. Since the DMA tests are limited in frequency range, Time–Temperature Superposition Principle (TTSP) is applied aiming at building the master curve of the rubber up to $10^6$ Hz and the four parameters constituting the Fractional Derivative Model (FDM) are identified from the master curve by using a least square method [7] and accounted in the structural part of the FEM vibro-acoustic model.

Two coupled vibro-acoustic FEM models are built: (i) bare panel + sound box and (ii) VEM coated panel + sound box. The responses of the structure and the acoustic cavity to a unitary point excitation are computed at selected points distributed along the structural and acoustic subsystems. Aiming to validate the numerical models, dynamic tests are performed, by reproducing the same configurations as those modeled by FEM. The structural and acoustic responses are measured by accelerometers and microphones at the same geometrical observation points as those generated in the numerical models, being an impact hammer used to excite the system. Numerical vs. experimental comparisons are done and good agreement is obtained, despite a slight under-prediction of the structural damping. It is observed that the sound inside the sound box cavity reduces, due to the smaller sound radiation generated by the treated panel.

## 2. Vibro-acoustic modeling using FEM

### 2.1. FEM/FEM coupled model

In a coupled vibro-acoustic system, the fluid is comprised in a bounded acoustic domain $V$, of which the boundary surface $\Omega_a$ contains imposed boundary conditions as pressure $\Omega_p$, impedance $\Omega_z$ and velocity $\Omega_v$ as well as an elastic structural surface $\Omega_s(\Omega_a = \Omega_s \cup \Omega_p \cup \Omega_v \cup \Omega_Z)$, as shows Fig. 1.

FE based models for vibro-acoustic problems are most commonly described in an Eulerian formulation, in which the fluid is described by a single scalar function, usually the acoustic pressure, while the structural components are described by a displacement vector. The resulting combined FE/FE model in the unknown structural displacements and acoustic pressures at the nodes of, respectively, the structural and the acoustic FE meshes are [8,9],

$$\left(\begin{bmatrix} K_s & K_c \\ 0 & K_a \end{bmatrix} + j\omega \begin{bmatrix} C_s & 0 \\ 0 & C_a \end{bmatrix} - \omega^2 \begin{bmatrix} M_s & 0 \\ -\rho_0 K_c^T & M_a \end{bmatrix}\right) \cdot \begin{Bmatrix} w_i \\ p_i \end{Bmatrix} = \begin{Bmatrix} F_{si} \\ F_{ai} \end{Bmatrix} \tag{1}$$

where $[\boldsymbol{K}_c]$ is the cross-coupling matrix in the coupled stiffness matrix and $[-\rho_0 \boldsymbol{K}_c^T]$ is the cross-coupling matrix in the coupled mass matrix.

In comparison with a purely structural or purely acoustic FE model, the coupled stiffness and mass matrices are no longer symmetrical due to the fact that the force loading of the fluid on the structure is proportional to the pressure, resulting in a cross-coupling term $K_c$ in the coupled stiffness matrix, while the force loading of the structure on the fluid is proportional to the acceleration, resulting in a cross-coupling term $M_c = -\rho K_c^T$ in the coupled mass matrix [8,9].

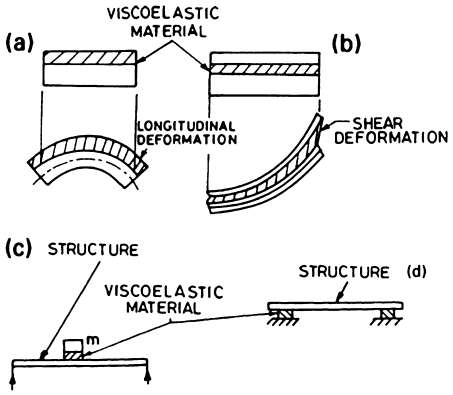


**Fig. 2.** (a) Unconstrained, (b) constrained, (c) tuned damper, (d) support damper.

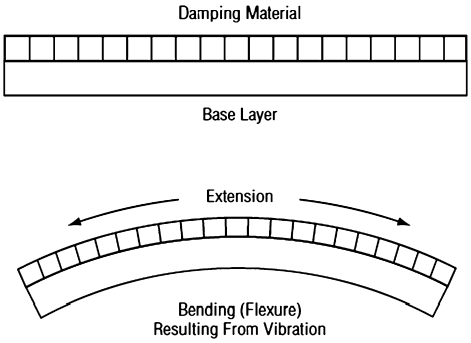


**Fig. 3.** Free-layer or unconstrained configuration.

### 2.2. Viscoelastic material

VEM treatments are well established and widespread around different areas as automotive, aerospace and naval, becoming a means of passively controlling structural vibrations and/or noise radiation. The practical use in aerospace industry is to apply weight-efficient forms of VEM assemblage configurations as shown in Fig. 2. These materials are constituted by long-range molecular order and exhibit a rheological behavior between that of a crystalline solid and a simple liquid [10]. Of particular importance is the dependency of both stiffness and damping on frequency and temperature [11].

Unconstrained damping treatments are the simplest form of inserting vibration damping and consist in attaching a VEM layer to an elastic structure. The extension and compression of the material under flexural stress from the elastic structure causes the cyclic deformation of the VEM. As consequence, the energy transferred to the core layer is dissipated to the exterior as heat (Figs. 2a and 3). The dissipative capacity of the VEM is associated with its capacity of storing strain energy. In the case of constrained-layer damping arrangement (Fig. 2b), the VEM is constrained between the elastic structure and a constraining layer, and shear strain is induced in the VEM during flexural vibrations.

Many researchers have devoted themselves to describe and characterize VEM. Ungar [12] assessed the definition of the loss factor in terms of energy quantities, in particular when it applies to composite VEM systems. Bert [10] reviews material damping and presents various measures of damping proposed for homogeneous materials. Furthermore, the two-parameter Maxwell and Kelvin–Voigt models are described as the starting point for derivations of more realistic models such as the Generalized Maxwell model, the Kelvin chain model, the Biot model, and the Fractional Derivative Model.

Structural damping models based on the linear theory of viscoelasticity assumes a relation between stress and strain based on the Boltzmann's principle. Being $\sigma_{ij}(t)$ and $\varepsilon_{ij}(t)$, respectively, the stress and strain tensors at time $t$, with $\dot{\varepsilon}_{ij}(t)$ the time derivative of the strain tensor, the stress–strain constitutive equation in time domain can be written as [13]:

$$\sigma_{ij}(t) = E_{ijkh}(0)\varepsilon_{kh}(t) + \int_0^{\infty} \dot{E}_{ijkh}(\tau)\varepsilon_{kh}(t-\tau)\mathrm{d}\tau \tag{2}$$

where $\sigma_{ij}(t) = 0$ and $\varepsilon(t) = 0$, for $t \leq 0$. $E_{ijkh}(t)$ are called relaxation functions and $E_{ijkh}(0)$ is the initial elasticity tensor. The relaxation functions are defined on $[0, +\infty[$, are differentiable with respect to $t$ on $[0, +\infty[$, their derivatives are $\dot{E}_{ijkh}(t)$ and are assumed to be integrated on $[0, +\infty[$. The relaxation functions can be written as:

$$E_{ijkh}(t) = E_{ijkh}(0) + \int_0^{\infty} \dot{E}_{ijkh}(\tau)\mathrm{d}\tau \tag{3}$$

Therefore, the limit of $E_{ijkh}(t)$, denoted as $E_{ijkh}(\infty)$, is finite as $t$ tends to $+\infty$. The tensor $E_{ijkh}(\infty)$ is called the equilibrium modulus and corresponds to the usual elastic coefficients of the elastic material for a static deformation (static equilibrium state is obtained as $t$ tends to infinity).

If the real functions $e_{ijkh}(t)$ are introduced, such that:

$$\begin{aligned} &e_{ijkh}(t) = 0 \quad \text{if } t < 0 \\ &e_{ijkh}(t) = \dot{E}_{ijkh}(t) \quad \text{if } t \geq 0 \end{aligned} \tag{4}$$

Since $e_{ijkh}(t) = 0$ for $t < 0$, one deduces that $e_{ijkh}(t)$ is a causal function. Using equation (4), the equation (2) can be written as:

$$\sigma_{ij}(t) = E_{ijkh}(0)\varepsilon_{kh}(t) + \int_{-\infty}^{\infty} e_{ijkh}(\tau)\varepsilon_{kh}(t-\tau)\mathrm{d}\tau \tag{5}$$

Equation (5) describes the most general formulation in the time domain within the framework of the linear theory of viscoelasticity. The usual approach of the one-dimensional stress–strain constitutive relationship that consists in modeling the equation in time domain by a linear differential equation in $\sigma(t)$ and $\varepsilon(t)$ corresponds to a particular case, which is an approximation of the general equation (5).

Several models exist to describe the time (or frequency) dependence of VEM properties. Among them, the Fractional Derivative Model (FDM), which describes the frequency-dependent modulus in the broadband rheological behavior of the material is described as:

$$E^*(\omega) = \frac{E_e + E_g(\mathrm{j}\omega\rho)^{\alpha}}{1 + (\mathrm{j}\omega\rho)^{\alpha}} \tag{6}$$

$E_e$: rubbery or long time modulus; $E_g$ is the glassy modulus; $\rho$ is the relaxation time, $\alpha$ is a constant related to the peak widening of loss factor. These four parameters can be identified from experimental master curves [7].

Therefore, the complex modulus can be expressed in the frequency domain as:

$$E^*(\omega) = E'(\omega) + \mathrm{j}E''(\omega), \quad \text{for uniaxial strain conditions} \tag{7a}$$

$$G^*(\omega) = G'(\omega) + \mathrm{j}G''(\omega), \quad \text{for shear strain conditions} \tag{7b}$$

The loss factor $\eta(\omega)$ may be defined as the non-dimensional quantity relating the imaginary and the real part of the complex modulus as:

$$\eta(\omega) = \frac{E''(\omega)}{E'(\omega)}, \quad \text{uniaxial strain} \tag{8a}$$

$$\eta(\omega) = \frac{G''(\omega)}{G'(\omega)}, \quad \text{shear strain} \tag{8b}$$

## 3. Modeling the vibro-acoustic systems (panels + sound box)

Two coupled models are built: (i) bare panel + sound box cavity (a cabin-like testing environment built to exploit both for noise transmission and noise insulation characterization of lightweight materials) and (ii) VEM coated panel + sound box cavity. Unitary excitation was applied at the center of the panels and transfer functions (acceleration/force and sound pressure level/force) are calculated up to 1,000 Hz. Fig. 4 shows the dimensions of the sound box as well as the set-up of the structural assemblage on the box.

### 3.1. Bare panel + sound box

A vibro-acoustic system, consisting of an aluminum (AL 5754) homogeneous plate of dimensions 0.443 m × 0.617 m × 0.003 m and the sound box acoustic cavity (Fig. 2) is modeled in COMSOL Multiphysics version 4.3b, using FEM. The geometrical coordinates of the sound box is described in Table 1. More detailed descriptions about the KU Leuven-PMA Sound Box can be seen in [14]. Table 2 describes the main aluminum characteristics, assigned as structural material, while for the acoustic part, one assigned the air at 20 °C as material.

At least 10 elements by wavelength were considered to build the FEM vibro-acoustic mesh. The finer mesh option was chosen, which yielded 53,759 free tetrahedral elements (minimum and maximum element sizes of 0.0046 and 0.0633 m, respectively, giving minimum and maximum analysis frequencies of 5,000 Hz and 12,000 Hz, approximately). The front wall

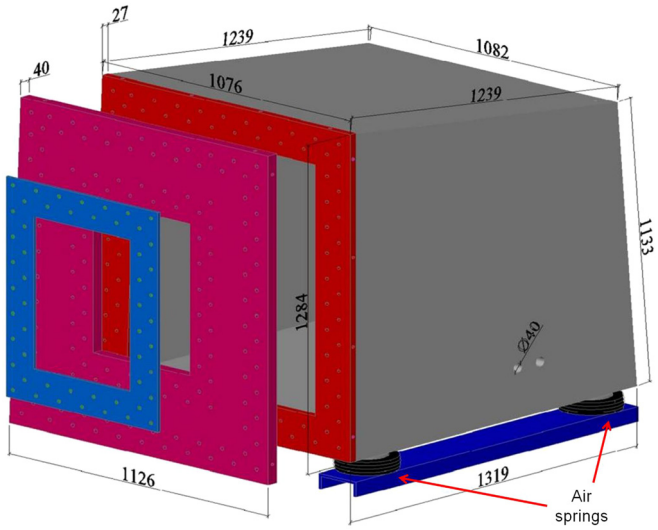


**Fig. 4.** A sketch of the experimental set-up geometry (dimensions in mm) [12].

**Table 1**
KU Leuven-PMA Sound Box geometry.

| Point | Coord. *X* | Coord. *Y* | Coord. *Z* |
|---|---|---|---|
| 1 | 0 | 0 | 0 |
| 2 | 0 | 0.815 | 0 |
| 3 | 1.15 | 0.815 | 0 |
| 4 | 1.15 | 0 | 0 |
| 5 | 0 | 0.001 | 0.982 |
| 6 | 0 | 0.778 | 0.981 |
| 7 | 1.082 | 0.783 | 0.848 |
| 8 | 1.082 | 0 | 0.849 |

**Table 2**
Al 5754 material characteristics.

| Aluminum AL5754 | |
|---|---|
| Density | 2700 kg/m$^3$ |
| Young's modulus | 70e–9 N/m$^2$ |
| Poisson's ratio | 0.33 |

of the vibro-acoustic system was modeled, with a symmetrically positioned A2 footprint area window, where the bare panel was positioned. The clamped boundary condition was applied at all edges of the aluminum panel, while the walls of the sound box were considered as rigid. Figs. 5a and 5b show the generated geometry and the respective FE mesh.

In view of assessing the structural responses, observation points were generated along the structural panel and inside the sound box. The coupled modal analysis was calculated to determine the first 200 modes (up to 1,570 Hz, approximately) of this vibro-acoustic system. Furthermore, an excitation of 1 N was applied in the middle of the plate, allowing us to calculate the transfer functions (acceleration/force and pressure/force) up to 1,000 Hz, in steps of 1 Hz, using the modal superposition principle.

### 3.2. *VEM coated panel + sound box*

The FDM, described in section 2.2, is used to simulate the VEM insertion on the aluminum homogeneous plate, studied as the structural part of a vibro-acoustic system. Before proceeding with the vibro-acoustic modeling, the VEM compound added to the aluminum panel must be characterized. In order to well represent the shear modulus of the referred self-adhesive rubber, Dynamic Mechanical Analysis (DMA) test campaigns were performed and the rubber master curve was built. As a consequence, the four FDM parameters to be considered in equation (6) were identified, as described in Table 3. Experimental vs. FDM master curves comparison is done and the good correlation verified in Fig. 6 is a fair indication that these parameters can represent the VEM shear behavior in the FEM model of the sandwich structure [7].

As a second step, the structural behavior of the sandwich panel (VEM + aluminum panel) was assessed by using FEM models, where the FDM parameters (identified by DMA) were considered to model the shear behavior of the constrained

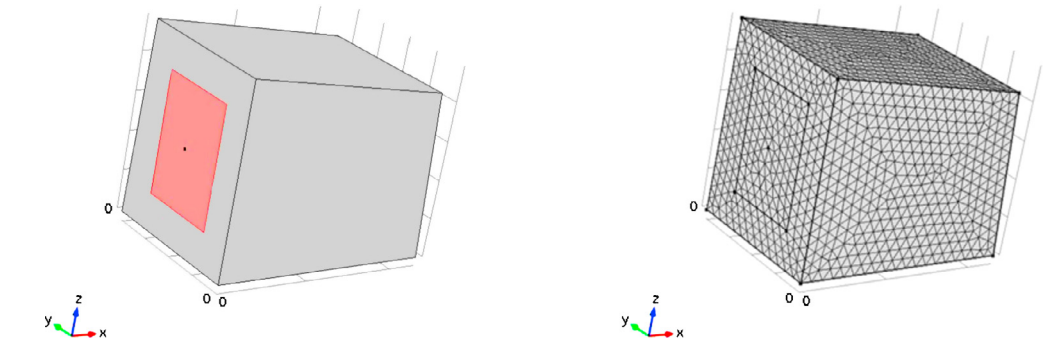

(a) Vibro-acoustic system (bare panel + acoustic cavity)

(b) Coupled vibro-acoustic mesh

**Fig. 5.** Sandwich panel + KU Leuven-PMA Sound Box.

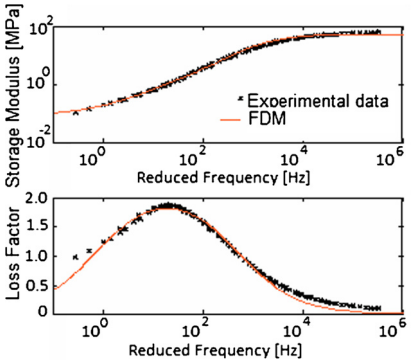


**Fig. 6.** Master curves of the self-adhesive synthetic rubber at 20 °C fitted by a FDM.

**Table 3**
FDM parameters.

| | |
|---|---|
| Relaxed modulus $G_e$ | 9.87e–4 Pa |
| Unrelaxed modulus $G_g$ | 6.06e–7 Pa |
| Relaxation time $\rho$ | 9.85e–5 s |
| Order of derivation $\alpha$ | 0.70 |

VEM layer up to 1,000 Hz, in different panel treatments and boundary conditions. In addition, an extensive experimental campaign was carried out to validate these pure structural models, in which experimental set-ups were assembled to simulate the same numerical model configurations built by FEM. Numerical vs. experimental comparisons were done and, despite slight under predictions of damping by the FEM models, good agreement was achieved [7].

The sandwich structure is composed of a homogeneous aluminum panel of dimensions 0.66 m × 0.86 m × 0.003 m, coated with a constrained VEM layer over an A2 footprint area (0.42 m × 0.594 m × 0.0015 m), and the damping treatment consists of a 1.373-mm-thick VEM layer, constrained by a 127-µm-thick aluminum layer, as shows Fig. 7a. Notice in Fig. 7b that 52 holes provide the sandwich panel coupling with a rigid frame and, as consequence, with the sound box cavity, where only the coated area (Fig. 7a) is the elastic structural surface in contact with the fluid of the acoustic cavity.

The modeling of sandwich structures is challenging: due to the strong variations of in-plane strains through the thickness of the core layer, shell elements cannot be used to model the VEM layer. A classical approach is to consider shell elements for the stiff elastic layers (i.e. the base plate and the constraining layer) and solid elements for the core layer of the VEM, as depicted in Fig. 8.

The frequency-dependent shear modulus of the VEM layer is described by FDM, whose identified parameters are given in Table 3, while a constant Poisson's ratio $\nu = 0.45$ is assumed and the density of the VEM is 1,100 kg/m$^3$. FDM can be introduced in COMSOL through the analytical expression of the complex frequency-dependent shear modulus (Eq. (6)). On the other side, the material properties of the AL5754 constituting the base panel and the constraining layer are given in Table 2.

The vibro-acoustic system is, therefore, built by clamping the sandwich panel to the sound box. The clamped boundary condition has significant impact on the dynamic response of lightweight panels. In such an assemblage configuration, local stresses are added to the structure, impacting its behavior. Test campaigns of different configurations of purely structural

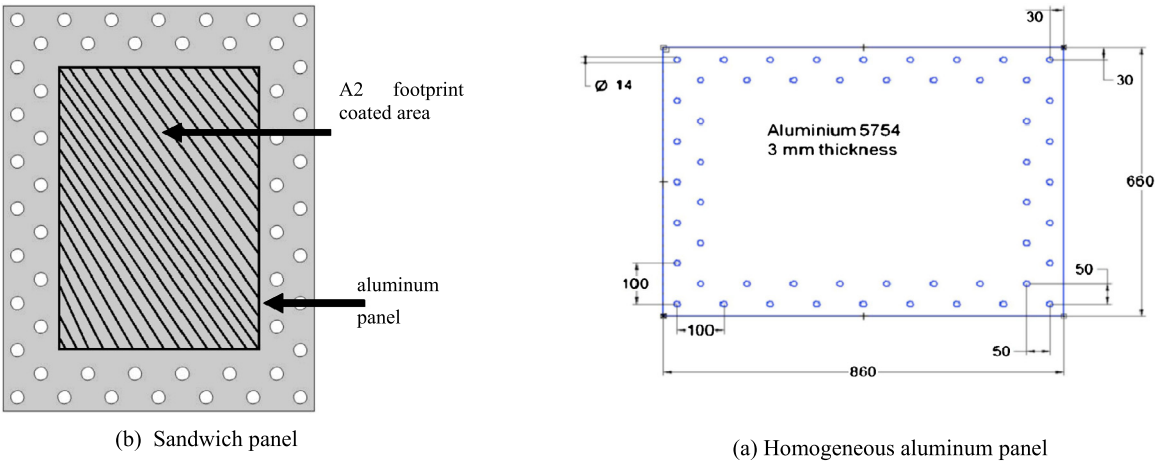


**Fig. 7.** Geometry of the sandwich panel.

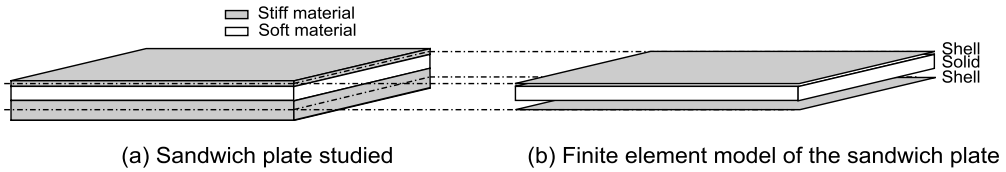


**Fig. 8.** Modeling of the sandwich plate.

coated panels were carried out to build a benchmark for lightweight structures numerical validations. Such model validations have shown that numerical vs. experimental comparisons present disagreements in the natural frequencies of around 10%, when the A2 footprint area (0.420 × 0.594 m) dimensions are considered in the FE models [7]. A more detailed evaluation of the assemblage set up shows that the mounting frame effect on the panel response is not accounted when the model of the A2 footprint dimensions panel is considered [14]. In this way, a model updating was done to better represent the clamped boundary condition in the panel assemblage configuration. Different panel dimensions were assessed and a good updating condition was obtained by increasing the panel geometry to 0.443 × 0.617 m, instead of 0.420 × 0.594 m and keeping the A2 footprint VEM coated area (0.420 m × 0.594 m).

The acoustic cavity was built up by adopting the sound box geometry (Table 1) and the assigned acoustic environment is the air at 20 °C (mass density 1.225 kg/m$^3$ and speed of sound 343 m/s). At least ten elements by wavelength were considered, and the finer mesh option was chosen, which yielded 53,682 elements (minimum and maximum element sizes of 0.00461 and 0.0634 m, respectively), with 83,476 degrees of freedom.

In the same way, as done in section 3.1, the front wall of the vibro-acoustic system was modeled, with a symmetrically positioned A2 footprint area window, where the updated sandwich panel was added. The clamping condition was applied at all edges of the base plate (the VEM and constraining layer were modeled as free boundary condition), while the walls of the sound box were considered as rigid. Fig. 9a shows the vibro-acoustic FEM mesh.

In view of assessing the structural and acoustic responses, observation points were generated along the structural panel and inside the cavity of the sound box (Fig. 9b). A point excitation of 1 N was applied in the middle of the panel, allowing calculating the transfer functions at the observation points. Frequency response analysis was done up to 1,000 Hz, in steps of 1 Hz, using the direct frequency response method.

## 4. Experimental validation

In order to validate the vibro-acoustic FEM models, an experimental campaign was conducted, where two set-ups were built to simulate the numerical models described in sections 3.1 and 3.2. The bare and sandwich panels were attached to the front wall of the KU Leuven-PMA Sound Box. Afterwards, the attachment was done by positioning the structural set (front wall + panel + frame) close to the open part of the Sound Box. Notice that the panel geometry in contact with the inner cavity is nominally identical to a width of 0.420 m and a length of 0.594 m, for an A2 footprint area. Accelerometers and microphones were installed at the same positions as those observation points generated in the numerical models. The system excitation, in the middle of the structural panel, was provided by an impact hammer. This hammer is equipped with a force transducer, which measured the transient input signal. Fig. 10a shows the base plate and the coated A2 footprint area, while Fig. 10b shows the referred sandwich panel attached to the KU Leuven-PMA Sound Box.

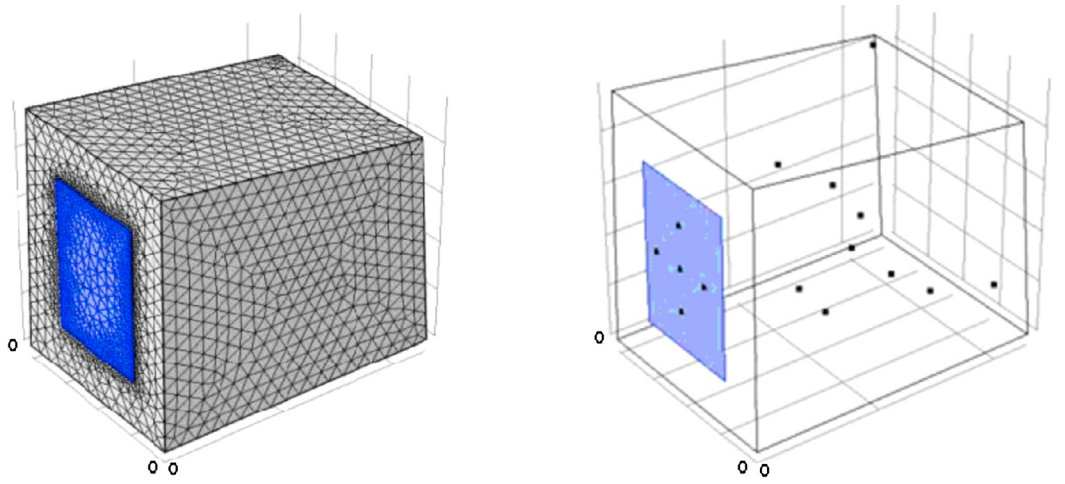

(a) Coupled vibro-acoustic mesh (b) Structural-acoustic observation points

**Fig. 9.** Vibro-acoustic mesh and observation points.

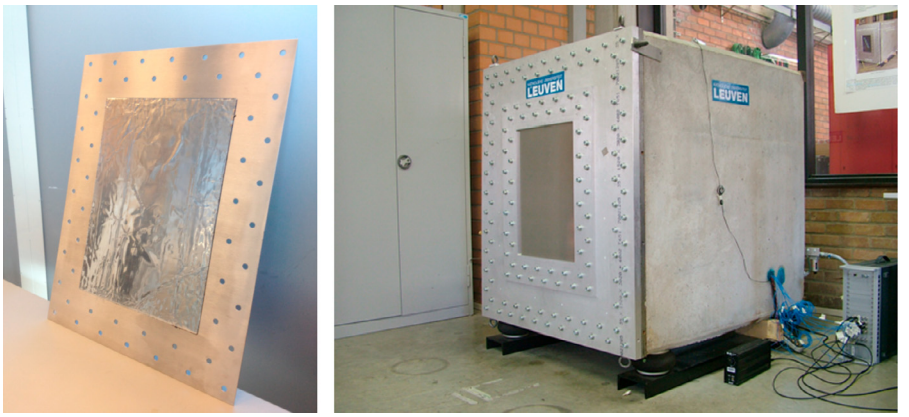


(a) Coated panel (b) Coated panel + KU Leuven - PMA Sound Box

**Fig. 10.** Sandwich structure (A2 footprint area) and vibro-acoustic system.

The panels were instrumented with five accelerometers (Fig. 11a), which captured the structural responses and allowed calculating the transfer functions between structural responses and excitation. For the acoustic part, the inner cavity responses were gathered by ten microphones, installed as shown in Fig. 11b. Both, structural and acoustic transfer functions, were measured up to 1,000 Hz.

## 5. Analyses and results

In the sections below, the structural and acoustic responses for numerical and experimental models are discussed. Transfer functions ((g/N) for structural part and (dB/N) for acoustic part) are presented and the damping insertion effect is assessed by comparing the structural and acoustic responses of the bare and coated panel configurations. Model validations are also done by numerical vs. experimental comparisons.

### *5.1. Bare panel + sound box*

Uncoupled and coupled numerical modal analyses were done to investigate the vibro-acoustic behavior of the set bare panel + sound box. The coupled modal analysis shows that additional modes corresponding to the coupling of the elastic part (panel) are present in this model. The simple frequency comparisons with pure (uncoupled) structural and acoustic modal analyses show the influence of the coupling in the panel as well as the cavity responses.

Table 4 presents the eight first frequencies calculated for purely structural, purely acoustic and coupled modal analyses. It is worthy to highlight that differences in the structural natural frequencies of the coupled vibro-acoustic model are noticed, in comparison with a simple structural model, due to the coupling effect. As an example, see that the first structural bending

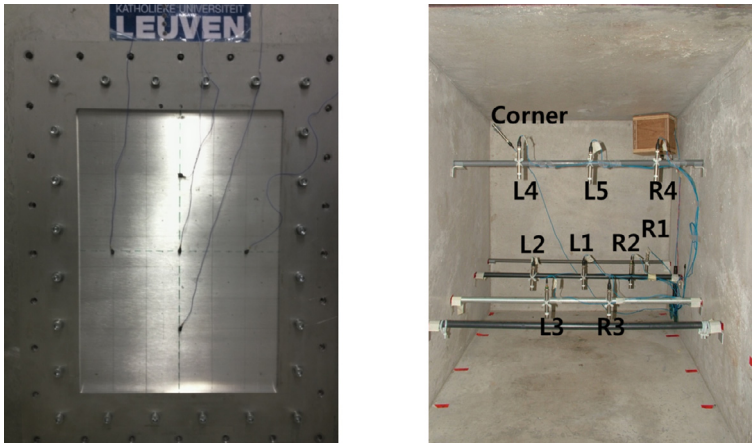


(a) Accelerometers (bare and coated panels) (b) Microphones inside the sound box cavitiy

**Fig. 11.** Structural (accelerometers) and acoustic (microphones) sensors positions.

**Table 4**
Purely structural vs. purely acoustic vs. coupled modal analyses.

| | Frequency (Hz) | | |
|---|---|---|---|
| | Structural modal analysis | Acoustic modal analysis | Coupled modal analysis |
| 1 | 106.03 | 1.32e–5 | 2.15e–5 |
| 2 | 172.43 | 152.29 | 103.55 |
| 3 | 253.36 | 186.95 | 152.85 |
| 4 | 282.70 | 213.74 | 167.97 |
| 5 | 314.70 | 242.22 | 185.72 |
| 6 | 418.61 | 262.41 | 212.27 |
| 7 | 433.77 | 284.08 | 243.15 |
| 8 | 476.60 | 307.42 | 245.84 |

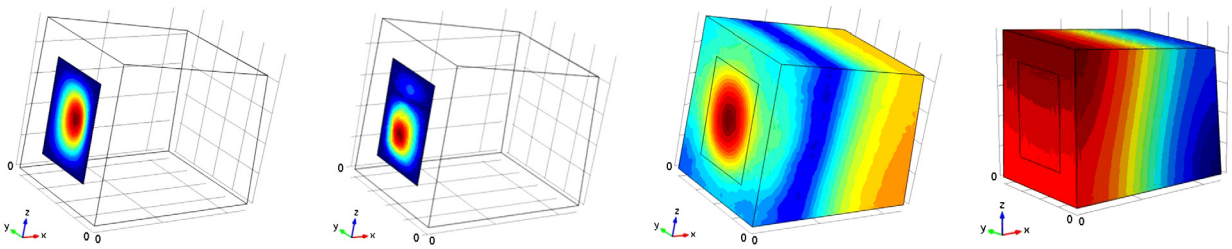

(a) 1st bending mode at 103.5 Hz (b) coupled structural mode at 152.8 Hz (d+a) (c) coupled acoustic mode at 103.5 Hz (a+d) (d)1st acoustic mode at 152.8 Hz

**Fig. 12.** Structural and acoustic modes.

mode is found at 106.03 Hz for the uncoupled analysis, while for the coupled modal analysis this first bending mode is at 103.55 Hz. For the acoustic cavity, the uncoupled and coupled models present the rigid Bode acoustic modes, once both models represent the closed sound box cavity. Furthermore, notice, in the coupled modal analysis, the influence of the acoustic oscillations on the structural responses and vice-versa, due to the coupling effect.

Fig. 12 shows the coupled numerical modes, calculated by modal analysis. See in Fig. 12b the influence of the acoustic mode at 152.8 Hz on the panel response. On the other side, Fig. 12c shows the impact of the structural displacements at 103.5 Hz on the cavity's acoustic pressure.

The FRF calculated by the numerical model are compared with those measured during the experimental campaign (see section 4). Fig. 13, shows the comparisons for both, structural (at accelerometer P5) and acoustic parts (at microphone L4).

The visual analysis of the Fig. 13a shows the impact of the acoustic pressure oscillations on the structural responses as seen at 152.29 Hz and 186.95 Hz. See that the coupling effect is more pronounced in the numerical model (black curve). One can still notice in Fig. 13a that the panel comparison responses present the same shape in the low-frequency range, with differences above 450 Hz. However, the magnitudes are not in good agreement, even in the low-frequency ranges.

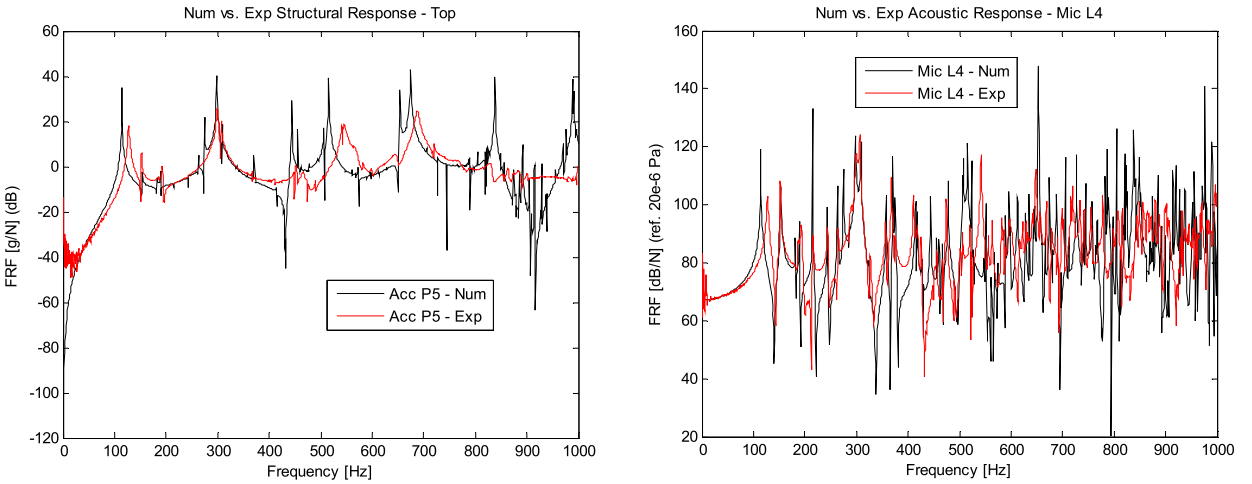


(a) FRF structural comparison at acc. P5

(b) FRF acoustic comparison at mic. L4

**Fig. 13.** Numerical vs. experimental comparisons.

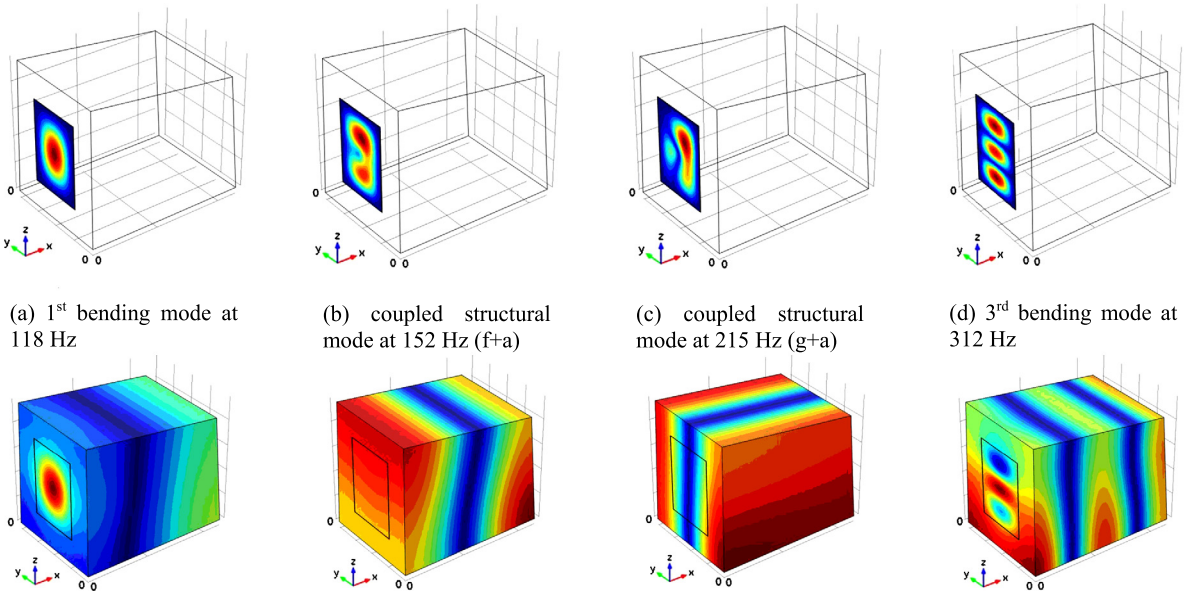

(a) 1st bending mode at 118 Hz

(b) coupled structural mode at 152 Hz (f+a)

(c) coupled structural mode at 215 Hz (g+a)

(d) 3rd bending mode at 312 Hz

(e) coupled acoustic mode at 118 Hz (a+f)

(f) 1st acoustic mode at 152 Hz

(g) 2nd acoustic mode at 215 Hz

(h) coupled acoustic mode at 312 Hz (d+f)

**Fig. 14.** Structural and acoustic modes.

Concerning the acoustic responses, the comparisons are pretty acceptable up to 500 Hz, with high modal density above this frequency range, as seen in Fig. 13b. Notice in this figure that the acoustic modes, at frequencies 152.8 Hz, 186.95 Hz and 307.42 Hz, present good agreement. On the other side, at 213.74 Hz, one notices a big difference in the pressure magnitude.

A better approximation of these numerical vs. experimental comparisons could be obtained by updating the vibro-acoustic model, rather than a purely structural model updating, as described in section 3.2.

### *5.2. Coated panel + sound box*

In section 3.2, the frequency response analysis was calculated up to 1,000 Hz, in steps of 1 Hz. Fig. 14 shows the deformed shapes corresponding to the sandwich panel vibration and cavity modes. Notice in Figs. 14b and 14c the influence of the acoustic oscillations on the structural responses, at 152 Hz and 215 Hz, respectively. Pure structural bending modes are illustrated in Figs. 14a and 13d (modes (1,1) and (1,3), respectively). On the other side, the influence of the structural

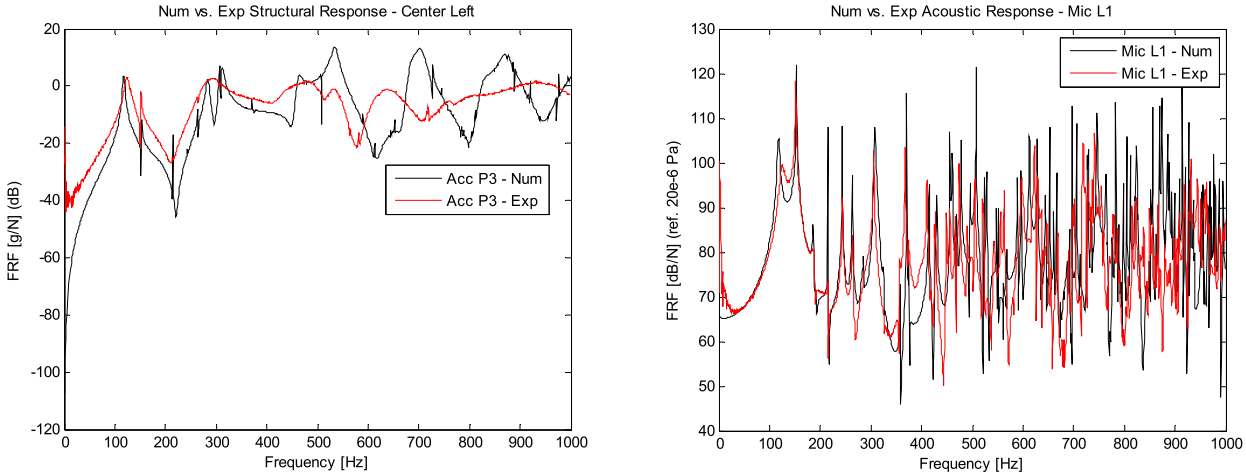


(a) FRF structural comparison at acc. P3

(b) FRF acoustic comparison at mic. L1

**Fig. 15.** Numerical vs. experimental comparisons.

displacements on the cavity responses are shown in Figs. 14e and 14h, at 118 Hz and 312 Hz, respectively. The pure acoustic longitudinal modes on planes $YZ$ and $XZ$ are shown in Figs. 14f and 14g, respectively.

Fig. 15, shows the numerical vs. experimental comparisons for both, structural (at accelerometer P3) and acoustic parts (at microphone L1). As for the bare panel (section 3.1), the frequencies regarding the acoustic modes affect the structural responses (Fig. 15a), with more pronounced effect in the numerical model (black curve). Notice in this figure that the shear modulus behavior of VEM constrained layers with FDM is not well seized in higher frequencies. As recommended in section 5.1, these numerical vs. experimental comparisons could be improved by updating the vibro-acoustic model. Notice in Fig. 15a that only the frequencies up to 300 Hz present acceptable correlation.

For the acoustic responses (Fig. 15b), the comparisons are acceptable up to 450 Hz, with a significant difference in magnitude at 215 Hz, where the measured response is much smaller. Above 450 Hz, the high modal density suggests a statistical analysis to assess the numerical vs. experimental agreement; however, a qualitative analysis shows that the differences are more evident from 800 Hz to 950 Hz.

In comparison with the bare panel + sound box configuration, the coated panel + sound box model presents frequency shifts, due to the constrained VEM layer addition. As an example, the first bending mode of the set bare panel + sound box is found at 103.5 Hz, while for the coated panel + sound box the first bending mode is at 118 Hz, approximately. This suggests that the VEM addition, in temperatures around 20 °C, has a stiffness-driven effect, rather than an added-mass effect as one could usually expect.

Fig. 16 presents the effect of the damping addition on the structural and acoustic responses, for both, numerical and experimental surveys. Comparisons are done for the bare plate and coated panel configurations.

Notice in Figs. 16a and 16b that the damping insertion reduces significantly the structural displacements, yielding smaller radiation to the acoustic cavity. In addition, see that high-frequency structural response attenuations are more pronounced, making the constraining layer dampers effective tools to control structural vibrations. See that peak attenuations of around 20 dB are obtained.

For the acoustic part, numerical and experimental models present sound pressure level reductions as seen in Figs. 16c to 16d. Observe the first acoustic coupled frequency (at 118 Hz) and see that a noise reduction of 20 dB, approximately, is obtained with the coated panel. A visual analysis over the whole frequency range shows the overall noise reduction inside the sound box, evidencing that VEM can be a complementary control technique (to porous-elastic materials) to attenuate internal sound pressure levels.

## 6. Conclusions

Coupled vibro-acoustic numerical models have been built to assess the effect of structural damping insertion with VEM on acoustic responses. The VEM was firstly characterized and the FDM was adopted to model the shear behavior of the constrained VEM applied on an aluminum homogeneous plate. The sandwich panel was attached to the acoustic model of the sound box. Structural and acoustic responses were calculated up to 1,000 Hz. In a second step, vibro-acoustic tests were done, with two experimental set ups, in which the lightweight panels (bare and sandwich) were connected to the KU Leuven – PMA Sound Box facility. These experimental set-ups allowed us to couple the vibro-acoustic subsystems and structural displacements and acoustic cavity responses up to 1,000 Hz were measured.

The coupling effect was verified in both elastic and acoustic sub-systems (Figs. 12 and 14), being the numerical model more sensible to this effect, as seen in Fig. 13a.

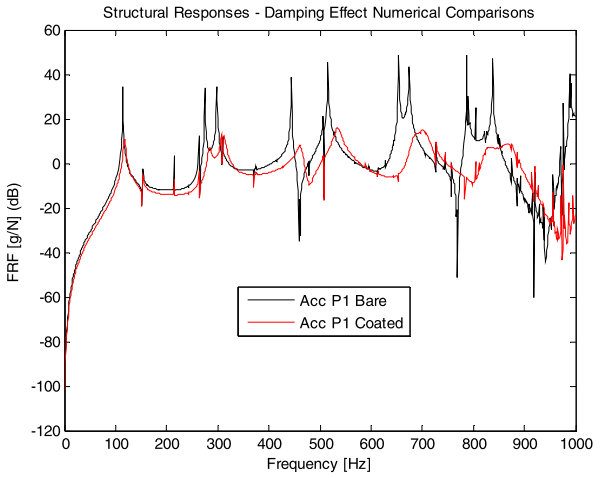


(a) Damping effect at P1 (numerical)

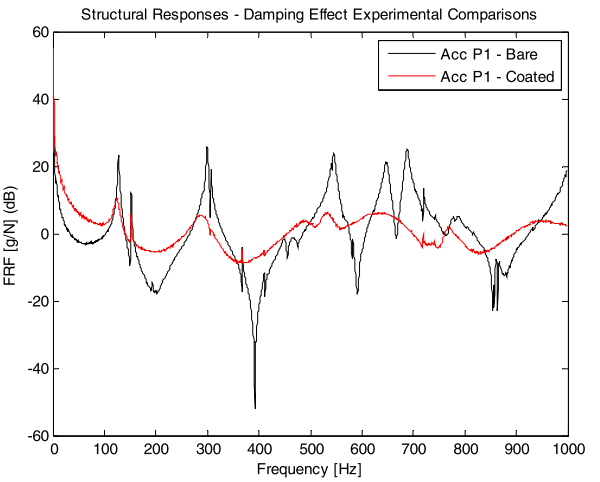


(b) Damping effect at P1 (experimental)

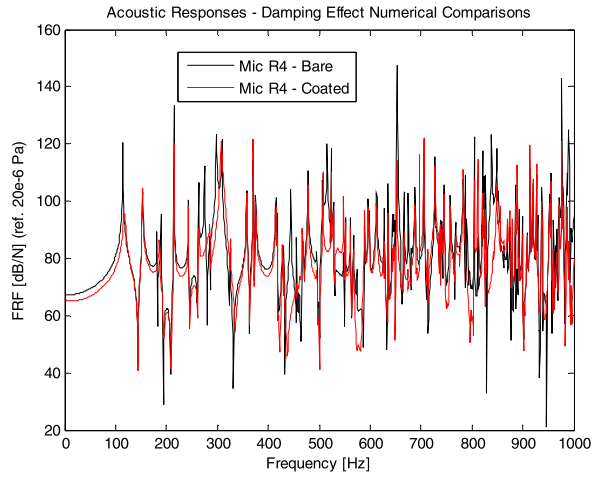


(c) Damping effect at Mic R4 (numerical)

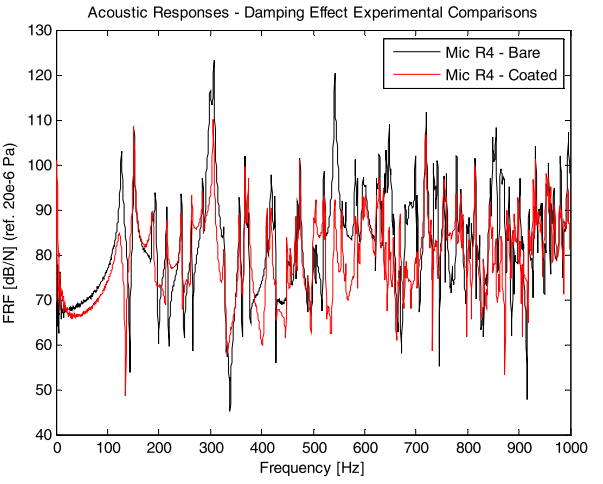


(d) Damping effect at Mic R4 (experimental)

**Fig. 16.** Damping effect comparisons (numerical and experimental).

Theoretical vs. experimental comparisons were done and acceptable agreement was observed for the acoustic part. On the other side, the structural part presented differences, showing that the FDM under-predicts the added damping, mainly in the higher order modes.

Excellent vibration control of the constrained VEM panel was noticed, in higher frequencies (above 300 Hz), consequently generating lower sound radiation reduction. For the acoustic part, one observes that the cavity responses were attenuated, mainly due to the portion reduction concerning the structural vibration.

As an important passive control technique, the use of porous-elastic materials to reduce the transmission loss in launchers fairings is well known. However, the noise due to the structural vibration radiation remains a significant portion that may still be attenuated and, as a consequence, reduce fairings and the internal vibration of space compartments induced by acoustics and vibration. As an efficient passive control technique, VEM addition can be a complementary technique (to porous-elastic materials) to attenuate internal sound pressure levels and appropriate to be applied in space systems.

As the next steps, the vibro-acoustic model updating, presented in this work, may be done to improve the numerical vs. experimental comparisons. Furthermore, vibro-acoustic models of a space system with combined VEM and porous-elastic materials may be built.

## Acknowledgements

The Brazilian Science without Borders Program is acknowledged by the first author. The authors gratefully acknowledge SIM (Strategic Initiative Materials in Flanders) and VLAIO (Flanders Innovation & Entrepreneurship) for their support of the ICON project M3NVH, which is part of the research program MacroModelMat (M3).

## References

[1] O.C. Zienkiewicz, R.L. Taylor, The Finite Element Method – the Three Volume Set, 6th ed., Butterworth–Heinemann, 2005.
[2] O. Von Estorff, Boundary Elements in Acoustics: Advances and Applications (Applicable Mathematics Series), WIT Press, Southampton, UK, 2007.
[3] R.H. Lyon, R.G. DeJong, Theory and Application of Statistical Energy Analysis, 2nd edition, 1995.
[4] W. Desmet, A Wave Based Prediction Technique for Coupled Vibro-Acoustic Analysis, Ph.D. Thesis, Department of Mechanical Engineering, Faculty of Engineering, Katholieke Universiteit Leuven, Belgium, 1998.
[5] P.J. Shorter, R.S. Langley, Vibro-acoustic analysis of complex systems, J. Sound Vib. 288 (2005) 669–699.
[6] K. Menard, Dynamic Mechanical Analysis: A Practical Introduction, 2nd edition, CRC Press, Boca Raton, FL, USA, 2008.
[7] R. Pirk, L. Rouleau, W. Desmet, B. Pluymers, Validating the modeling of sandwich structures with constrained layer damping using fractional derivative models, J. Braz. Soc. Mech. Sci. Eng. 38 (2016) 1959, http://dx.doi.org/10.1007/s40430-016-0533-7.
[8] W. Desmet, P. Sas, Introduction to Numerical Acoustics, Notes of Grasmech Course, Department of Mechanical Engineering, Faculty of Engineering, Katholieke Universiteit Leuven, Belgium, 2001.
[9] R. Ohayon, C. Soize, Structural Acoustics and Vibrations, Academic Press, 1998.
[10] C.W. Bert, Material damping: an introductory review of mathematic measures and experimental techniques, J. Sound Vib. 29 (2) (1973) 129–153.
[11] S.W. Park, Analytical modeling of viscoelastic dampers for structural and vibration control, Int. J. Solids Struct. 38 (2001) 8065–8092.
[12] E.E. Ungar, Loss factors of viscoelastic systems in terms energy concepts, J. Acoust. Soc. Am. 34 (7) (1962) 954.
[13] R. Ohayon, C. Soize, Advanced Computational Vibroacoustics, Cambridge University Press, Cambridge, UK, 2014.
[14] M. Vivolo, Vibro-Acoustic Characterization of Lightweight Panels by Using a Small Cabin, Ph.D. Thesis, Department of Mechanical Engineering, Faculty of Engineering, Katholieke Universiteit Leuven, Belgium, 2013.